

Silencing of mitochondrial Lon protease deeply impairs mitochondrial proteome and function in colon cancer cells

Lara Gibellini,^{*,1} Marcello Pinti,^{†,1} Federica Boraldi,[†] Valentina Giorgio,[‡] Paolo Bernardi,[‡] Regina Bartolomeo,^{*} Milena Nasi,^{*} Sara De Biasi,^{*} Sonia Missiroli,[§] Gianluca Carnevale,^{*} Lorena Losi,[†] Anna Tesei,^{||} Paolo Pinton,[§] Daniela Quaglino,[†] and Andrea Cossarizza^{*,1,2}

^{*}Department of Surgery, Medicine, Dentistry, and Morphological Sciences, and [†]Department of Life Sciences, University of Modena and Reggio Emilia, Modena, Italy; [‡]Department of Biomedical Sciences, University of Padova, Padua, Italy; [§]Department of Morphology, Surgery, and Experimental Medicine, University of Ferrara, Ferrara, Italy; ^{||}Biosciences Laboratory, IRCCS Istituto Scientifico Romagnolo per lo Studio e la Cura dei Tumori (IRST), Meldola, Italy; ¹Dipartimento Sperimentale Interaziendale, Campus San Lazzaro, University of Modena and Reggio Emilia, Reggio Emilia, Italy

ABSTRACT Lon is a nuclear-encoded, mitochondrial protease that assists protein folding, degrades oxidized/damaged proteins, and participates in maintaining mtDNA levels. Here we show that Lon is up-regulated in several human cancers and that its silencing in RKO colon cancer cells causes profound alterations of mitochondrial proteome and function, and cell death. We silenced Lon in RKO cells by constitutive or inducible expression of Lon shRNA. Lon-silenced cells displayed altered levels of 39 mitochondrial proteins (26% related to stress response, 14.8% to ribosome assembly, 12.7% to oxidative phosphorylation, 8.5% to Krebs cycle, 6.3% to β -oxidation, and 14.7% to crista integrity, ketone body catabolism, and mtDNA maintenance), low levels of mtDNA transcripts, and reduced levels of oxidative phosphorylation complexes (with >90% reduction of complex I). Oxygen consumption rate decreased 7.5-fold in basal conditions, and ATP synthesis dropped from 0.25 ± 0.04

to 0.03 ± 0.001 nmol/mg proteins, in the presence of 2-deoxy-D-glucose. Hydrogen peroxide and mitochondrial superoxide anion levels increased by 3- and 1.3-fold, respectively. Mitochondria appeared fragmented, heterogeneous in size and shape, with dilated cristae, vacuoles, and electrondense inclusions. The triterpenoid 2-cyano-3,12-dioxooleana-1,9-dien-28-oic acid, a Lon inhibitor, partially mimics Lon silencing. In summary, Lon is essential for maintaining mitochondrial shape and function, and for survival of RKO cells.—Gibellini, L., Pinti, M., Boraldi, F., Giorgio, V., Bernardi, P., Bartolomeo, R., Nasi, M., De Biasi, S., Missiroli, S., Carnevale, G., Losi, L., Tesei, A., Pinton, P., Quaglino, D., Cossarizza, A. Silencing of mitochondrial Lon protease deeply impairs mitochondrial proteome and function in colon cancer cells. *FASEB J.* 28, 000–000 (2014). www.fasebj.org

Key Words: respiration • oxphos • RKO cells • mtDNA • mtRNA

Abbreviations: 2-DE, 2-dimensional gel electrophoresis; 2DG, 2-deoxy-D-glucose; ACN, acetonitrile; BSA, bovine serum albumin; CDDO, 2-cyano-3,12-dioxooleana-1,9-dien-28-oic acid; CRC, colorectal cancer; cyt *c*, cytochrome *c*; DAPI, 4',6-diamidino-2-phenylindole; DMEM, Dulbecco's modified Eagle's medium; doxy, doxycycline; DTT, dithiothreitol; EDTA, ethylenediaminetetraacetic acid; FBS, fetal bovine serum; FCCP, carbonyl cyanide-4-(trifluoromethoxy)phenylhydrazone; FSC, forward scatter; HRP, horseradish peroxidase; Lon, Lon protease; MALDI-TOF/TOF-MS, matrix-assisted laser desorption/ionization tandem time-of-flight mass spectrometry; MEM, minimum essential medium; MFI, mean fluorescence intensity; MMP, mitochondrial membrane potential; mtDNA, mitochondrial DNA; mtRNA, mitochondrial RNA; OCR, oxygen consumption rate; oxphos, oxidative phosphorylation; PARP, poly(ADP-ribose) polymerase; PBMNC, peripheral blood mononuclear cell; PBS, phosphate buffered saline; PMF, peptide mass fingerprinting; shCtrl, short hairpin RNA control; shLon, short hairpin RNA targeting Lon protease; shRNA, short hairpin RNA; SSC, side scatter; TMRM, tetramethylrhodamine, methyl ester; tTS, tetracycline transcriptional silencer

COLON CANCER REPRESENTS a major malignancy worldwide (1). Despite intensive efforts, the resistance to chemotherapy remains a main challenge, and an urgent need persists to find potential targets for novel drugs. Colon cancer cells often develop adaptive mechanisms to survive in a microenvironment where oxygen and nutrients are scarce, and require functionally active mitochondria to survive. As a consequence, such organelles have to adapt to the new environment, and their modified bioenergetic status can contribute to drug resis-

¹ These authors contributed equally to this work.

² Correspondence: Department of Surgery, Medicine, Dentistry, and Morphological Sciences, University of Modena and Reggio Emilia, Via Campi, 287, 41125 Modena, Italy. E-mail: andrea.cossarizza@unimore.it

doi: 10.1096/fj.14-255869

This article includes supplemental data. Please visit <http://www.fasebj.org> to obtain this information.

tance and tumor growth. While changes in glycolytic pathway induced by HIF-1 α have been widely investigated in colorectal cancer (CRC), less is known concerning alterations of mitochondrial functionality (2–5). Depletion of mitochondrial DNA (mtDNA) results in respiratory-deficient cells, which show decreased colony formation in soft agar, reduced tumor formation in nude mice, and increased sensitivity to cytotoxic drugs (6). Thus, even if changes occurring in colon cancer metabolism are not completely understood, mitochondria appear to be essential for tumor survival and growth.

Lon protease (Lon) is a nuclear-encoded, mitochondrial ATP-dependent protease ubiquitously expressed in human cells and tissues. Lon is homologue of yeast PIM1 protease (7) and, throughout evolution, has maintained the same functions, *i.e.*, to act as a protease and as a chaperone. Lon degrades oxidized and damaged proteins, including aconitase, and participates in the assembly and folding of regulatory proteins, including Cox4-1, StAR, ALAS-1, TFAM, and glutaminase C (8, 9). In addition, Lon binds mtDNA in a sequence- and strand-specific manner (10) and participates in mtDNA maintenance, either by interacting with DNA polymerase- γ or with the helicase Twinkle (11). As a regulator of mitochondrial functions, Lon is induced by several stressors, such as hypoxia, oxidative stress, ischemia, heat shock, serum starvation, and endoplasmic reticulum stress (12, 13), and its expression and activity are modulated in different pathologies (14–16).

To investigate the role of Lon in human colon cancer cells, we have silenced Lon mRNA and analyzed the modifications of mitochondrial proteome and mitochondrial functionality, along with cell proliferation and death in RKO cell line. Our data show that Lon is essential for the correct assembly and functionality of mitochondria respiratory chain, whose impairment alters the survival of colon cancer cells.

MATERIALS AND METHODS

Cell culture

RKO, HDLM-2, K562, PC3, and DU145 were cultured in RPMI medium supplemented with 10% fetal bovine serum (FBS) and gentamicin. SHSY5Y and MCF7 cells were maintained in Dulbecco's modified Eagle's medium (DMEM) supplemented with 10% fetal bovine serum and gentamicin. HEPG2 cells were cultured in minimum essential medium (MEM), supplemented with 10% FBS, 2 mM L-glutamine, vitamins, nonessential amino acids, and gentamicin. Cells were maintained in 5% CO₂ atmosphere at 37°C. When required, cells were maintained in condition of glucose deprivation by adding 2-deoxy-D-glucose (2DG; 80 mM) to complete medium. When indicated, hydrogen peroxide (H₂O₂; 400 μ M) was added to cell culture for 4 h to induce oxidative stress; the oleanane triterpenoid 2-cyano-3,12-dioxooleana-1,9-dien-28-oic acid (CDDO) was added to cell culture for 24 h at concentrations 0.1 and 1 μ M.

Peripheral blood mononuclear cells (PBMCs) were isolated by Ficoll-Hypaque density gradient according to standard procedures from 20 ml of venous blood collected into ethylenediaminetetraacetic acid (EDTA) tubes from each

donor, who gave informed consent. Next, 10⁷ PBMCs were incubated overnight in RPMI in the presence (then indicated as activated) or in the absence (then indicated as resting) of 2 μ g/ml anti-CD3 anti-CD28. PBMCs (9 \times 10⁷) were used to separate CD14⁺ and CD19⁺ cells by using CD14⁺ and CD19⁺ magnetic beads, respectively. CD14⁺ cells (1.8 \times 10⁷; then indicated as monocytes) and CD19⁺ (5 \times 10⁶; then indicated as B lymphocytes) were obtained and then cultured in RPMI medium. Monocytes were incubated overnight in the presence (then indicated as activated monocytes) or in the absence (then indicated as resting monocytes) of 0.5 μ g/ml lipopolysaccharide; whereas B lymphocytes were incubated in the presence (then indicated as activated B lymphocytes) or in the absence (then indicated as resting B lymphocytes) of 2 μ M CpG oligonucleotides for 72 h. At the end of the incubations, the presence of activated cells was evaluated by flow cytometry. In particular, PBMCs were stained with anti-CD4, anti-CD8, anti-HLA-DR, and anti-CD95 to analyze the amount of HLA-DR and CD95 double-positive cells. Activated monocytes and B lymphocytes were evaluated based on physical parameters. A minimum of 10⁶ cells/sample were acquired for the single cell analysis on Attune Acoustic Focusing Cytometer (Life Technologies Corp., Carlsbad, CA, USA). The instrument is equipped with a blue laser (488 nm, 20 mW, for detection of FITC, PE, ECD, and PE-Cy7 in this study) and a red laser (638 nm, 50 mW, for detection of APC and APC-H7), has 4 emission channels for the blue laser and 2 emission channels for the red laser, and allows up to 6-color analysis in addition to forward-scatter (FSC) and side-scatter (SSC) data collection. Data were acquired in list mode using Attune Cytometric 1.2.5 software and then analyzed by FlowJo 9.8.4 (TreeStar Inc., Ashland, OR, USA) under Mac OSX (Apple Inc., Cupertino, CA, USA). All culture media and culture reagents were from Life Technologies.

Tissue samples and protein extraction

Formalin-fixed paraffin-embedded (FFPE) tissues were from patients who underwent surgical resection of CRC and gave informed consent. Non-neoplastic (normal mucosa) colon tissues were excised from normal areas of surgical fragments placed distant to the tumor. FFPE microtome sections were deparaffinized according to the protocol reported in Addis *et al.* (17). Briefly, samples were deparaffinized by incubating at room temperature in xylene for 10 min and then centrifuged at 12,000 g for 3 min, and incubation/centrifugation steps were repeated two more times. The deparaffinized tissue pellets were then rehydrated with a graded series of ethanol (100, 95, 90, 70%, and H₂O). All samples were then weighed, and matched amounts of tissues were each immersed at a 20% w/v ratio in extraction buffer [20 mM Tris HCl, pH 8.8; 2% SDS; and 200 mM dithiothreitol (DTT)]. Samples were incubated at 100°C for 20 min and then at 80°C for 2 h with shaking. Extracts were centrifuged for 15 min at 12,000 g at 4°C, quantified by the Bradford assay, and then loaded on acrylamide/bisacrylamide precast gels.

Constructs, retrovirus preparation, and infection

The oligonucleotide 5'-GGGATCCGTTTCGTCTCGCCCA-GCCTTTTCAAGAGAAAGGCTGGGCGAGACGAACCTTTT-GAATTCCTT-3' was cloned into RNAi-Ready-pSiren-RetroQ-ZsGreen expression vector (Clontech, Mountain View, CA, USA), and RNAi-Ready-pSiren-RetroQ-TetP expression vector (Clontech), for constitutive and inducible expression of Lon short hairpin RNA (shRNA), respectively. With regard to constitutive down-regulation, the retroviral constructs RNAi-Ready-pSiren-RetroQ-ZsGreen-Lon and RNAi-Ready-pSiren-RetroQ-ZsGreen-

scramble were generated and used to infect RKO cells. Cells with the highest ZsGreen fluorescence were sorted by using a MoFlo XDP flow cytometer (Beckman Coulter, Fullerton, CA, USA) and then maintained in culture. With regard to inducible down-regulation, the retroviral construct RNAi-Ready-pSiren-RetroQ-TetP-Lon was generated that expresses Lon shRNA under the control of the tetracycline transcriptional silencer (tTS). pQC-tTS-In vector was used to generate stable tTS-expressing cells that were selected for G418 resistance, and several resistant clones were isolated and screened with pSiren-RetroQ-Tet-Luc luciferase vector to identify clones with low background and high shRNA induction. Stable tTS cells were infected with recombinant pSiren-RetroQ-TetP-Lon virus and selected with puromycin. Several colonies were picked up and expanded into mass culture and screened for doxycycline (doxy)-inducible expression of Lon. The analysis of Lon protein level was performed after induction of shRNA expression with doxy for 72 h or in parallel uninduced cultures.

Expression analysis

DNA and RNA were extracted from cells by using QIAmp DNA mini kit (Qiagen, Hilden, Germany) and RNeasy mini kit (Qiagen) following manufacturer's instructions. The following primers were used: mtDNA, forward 5'-CACAGAAGCTGCCATCAAGTA-3', reverse 5'-CCGGAGAGTATATTGTTGAAGAG-3'; gen, forward 5'-GGCTCTGTGAGGGATATAAAGACA-3', reverse 5'-CAAA-CCACCCGAGCAACTAATCT-3'; ND1, forward 5'-CCTTCGCTGACGCCATAAA-3', reverse 5'-CGGTGATGTAGAGGGT-GATG-3'; ND6, forward 5'-AACCCTGACCCCTCTCCTTC-3', reverse 5'-TGGAGGTAGGATTGGTGCTG-3'; cytB, forward 5'-AGTCCCACCCTCACAGATT-3', reverse 5'-TTGTTT-GATCCCGTTTCGTG-3'; L13, forward 5'-GCTGGAAGTACCAG-GCAGTGA-3', reverse 5'-ACCGGTAGTGGATCTTGGCTT-3'. Quantification of mtDNA and mitochondrial RNA (mtRNA) transcripts (ND1, ND6, cytB) was performed as described previously (18). Total cellular proteins were obtained by lysing cells with RIPA buffer (50 mM Tris, pH 7.5; 0.1% Nonidet P-40; 0.1% deoxycholate; 150 mM NaCl; 4 mM EDTA; and protease inhibitors). Total cellular protein (10–50 µg) was loaded in SDS-PAGE and, after gel electrophoresis, was transferred onto a nitrocellulose membrane. The membranes were incubated in the presence of primary antibody, washed, and incubated with a secondary antibody conjugated with horseradish peroxidase (HRP). HRP activity was detected using Immobilon Western Chemiluminescent HRP substrate (Millipore, Billerica, MA, USA). The blot was developed, and the densitometric analysis was performed using ImageJ (U.S. National Institutes of Health, Bethesda, MD, USA). The following antibodies were used: anti-TFAM (Abnova Corp., Taipei, Taiwan), anti-VDAC1/Porin (Abcam Inc., Cambridge, UK), MitoProfile Total Oxphos Human WB antibody cocktail (Abcam), anti-GAPDH (Trevigen, Gaithersburg, MD, USA), anti-GRP75 (Thermo Scientific, Waltham, MA, USA), anti-MDHM (Thermo Scientific), anti-EFTu (Novus Biologicals, Littleton, CO, USA), anti-UCRI (Novus Biologicals), anti-human mitochondrial protein (Millipore), anti-cytochrome *c* (Novus Biologicals), anti-cleaved caspase 9 (Cell Signaling Technology, Danvers, MA, USA), anti-poly-(ADP-ribose) polymerase (PARP; Santa Cruz Biotechnology, Dallas, TX, USA), goat anti-mouse IgG (Fc):HRP (Serotec, Kidlington, UK), goat anti-rabbit IgG (Fc):HRP (Serotec), goat anti-mouse F(ab')₂ Alexa546 (Life Technologies), and goat anti-rabbit F(ab')₂ Alexa647 (Life Technologies). Lon was probed using a custom anti-Lon polyclonal antibody (Primm, Milan, Italy) to the His-Tag recombinant protein Lon (from aa 376 to aa 497; QQR-LGREVEEKIKQTHRKYLLQEQLKIIKELGLEKDDKDAIEEKFERLKLKELVVPKHVMDVVDDELSKLGLLDNHSEFNVTRNYLDWLTSIPWGWKYSNENLDLARAQAVLEEDHYGMEDV).

Confocal microscopy

Cells were grown on glass coverslips. After treatment, cells were washed with phosphate buffered saline (PBS) and fixed with 4% paraformaldehyde in PBS for 15 min. Fixed monolayer cells were permeabilized with 0.1% Triton X-100 in PBS for 5 min and blocked with 3% bovine serum albumin (BSA) in PBS for 30 min, at room temperature. Then, samples were incubated with primary antibodies in PBS containing 3% BSA, for 1 h at room temperature. After washing in PBS containing 3% BSA, samples were incubated for 1 h at room temperature with secondary antibodies. After washing in PBS, samples were stained with 1 µg/ml 4',6-diamidino-2-phenylindole (DAPI) in PBS for 1 min and mounted with antifading medium (0.21 M Dabco and 90% glycerol in 0.02 M Tris, pH 8.0). Negative controls were samples not incubated with the primary antibody. The multilabeling immunofluorescence experiments were carried out avoiding cross-reactions between primary and secondary antibodies. Fluorescent samples were observed by a Nikon A1 confocal laser scanning microscope (Nikon, Tokyo, Japan) as described below. For multiple detection, the samples were sequentially excited with the respective laser wavelength: 405 nm lines of a diode laser for DAPI; 488 nm lines of the argon laser for ZsGreen; 543 nm lines of a HeNe laser for Alexa 546; and 637 nm lines of a diode laser for Alexa647. The excitation and detection of the samples were carried out in sequential mode to avoid overlapping of the two signals. Optical sections were obtained at increments of 0.5 µm in the *z* axis and were digitized with a scanning mode format of 1024 × 1024 pixels and 4096 gray levels. Spectral analysis was carried out to exclude overlapping between multiple signals. The confocal serial sections were processed with ImageJ software to obtain 3-dimensional projections, and image rendering was performed by Adobe Photoshop software (Adobe Systems, San Jose, CA, USA). Colocalization analysis was performed as described previously. Briefly, the 2-dimensional scatter plot diagram of each image was analyzed to evaluate the spatial colocalization of the signals, and the Pearson's correlation was calculated. For each scatter plot diagram, areas with the strongest colocalized signals, corresponding to pixels with intensity values > 2400 gray levels (on a scale from 0 to 4096) for both detectors, were selected to generate colocalization binary maps.

Transmission electron microscopy

Scraped cells were centrifuged at 10,000 *g* at 4°C for 5 min. Pellets were fixed overnight with 2.5% glutaraldehyde in Tyrode's buffer, postfixed for 2 h in 1% osmium tetroxide, dehydrated, and embedded in Spurr resin. Semithin sections obtained through the whole thickness of the pellets were stained with toluidine blue and observed with a Zeiss Axio-phot light microscope (Carl Zeiss, Oberkochen, Germany). Ultrathin sections were stained with uranyl acetate and lead citrate and observed with a JEM 2010 transmission electron microscope (Jeol, Tokyo, Japan).

Isolation of mitochondria

Cells were washed with PBS, trypsinized, suspended in 5 ml of ice-cold homogenization buffer (0.25 M sucrose, 0.25 mM ethylene glycol tetraacetic acid (EGTA), 5 mM 4-(2-hydroxyethyl)piperazine-1-ethanesulfonic acid (HEPES), 1 mM DTT, and protease inhibitor cocktail, pH 7.4), and disrupted by 10 strokes of a Teflon pestle in a glass homogenizer. The homogenization and subsequent steps were performed on ice. The homogenates were centrifuged at 1000 *g* for 10 min. The pellet was rehomogenized and centrifuged at 1000 *g*. The

combined supernatants were centrifuged at 17,000 *g* for 15 min. The pellet was resuspended in iodixanol (Optiprep; Sigma-Aldrich, St. Louis, MO, USA) diluted in homogenization buffer to obtain 36% iodixanol concentration. This fraction was layered with 30 and 10% iodixanol-containing homogenization buffer, and the gradient was centrifuged at 50,000 *g* for 4 h (SW41 Titanium swing-out rotor L-70 Ultracentrifuge; Beckman Coulter, Fullerton, CA, USA). Mitochondria were banded above the 10–30% interface and were collected by aspiration. The mitochondrial fraction was diluted 1:1 in ice-cold PBS and centrifuged at 14,000 rpm for 15 min in a benchtop centrifuge. The mitochondria pellets were washed again with 1 ml of PBS, centrifuged, frozen in liquid nitrogen, and stored at -80°C . All chemical reagents were from Sigma-Aldrich.

Sample preparation for 2-dimensional gel electrophoresis (2-DE)

The mitochondrial pellets, obtained as indicated above, were resuspended in 100 μl of 1% Triton X-100 and 2% SDS and solubilized by water-bath sonication. The mitochondrial pellets were subjected to sonication for 2 min in an ice-water bath by using a Branson LT9 sonifier (Gima, Milan, Italy). The sonication was repeated 3 \times after allowing the sample to cool down for 2 min in ice after each sonication. Then, the samples were incubated at 4°C for 30 min and treated with PlusOne 2-D Clean-Up Kit (GE Healthcare, Little Chalfont, UK). In the cleaning protocol, samples were left in wash buffer at -20°C for 24 h. Mitochondrial protein pellets were then resuspended in rehydration solution containing 7 M urea, 2 M thiourea, 2% 3-[(3-cholamidopropyl)dimethylammonio]-1-propane-sulfonate (CHAPS), 65 mM DTT, and 0.01% bromphenol blue, and protein concentration was determined by Bradford assay. 2-DE was carried out using the Immobiline polyacrylamide system (GE Healthcare), as described previously, on a preformed immobilized nonlinear pH gradient (pH 3–10, 18 cm length). Briefly, sample load was 60 μg /strip in analytical runs and 800 μg /strip in preparative gels. Isoelectric focusing was performed on the IPGphor system (GE Healthcare) at 16°C , using two different protocols. For analytical gels: passive rehydration for 16 h, 500 V for 1 h, 500–2000 V for 1 h, 3500 V for 3 h, from 3500 to 8000 V in 30 min, and 8000 V for 12 h. For preparative gels, a preliminary step at 200 V constant for 12 h was added. Thereafter, immobilized pH gradient strips were reduced (2% dithioerythritol) and alkylated (2.5% iodoacetamide) in equilibration buffer (6 M urea; 50 mM Tris-HCl, pH 6.8; 30% glycerol; and 2% SDS). When the equilibration phase was finished, strips were loaded onto 12% acrylamide vertical gels using an Ettan DALTsix electrophoresis unit (GE Healthcare). Analytical gels were stained with silver stain, whereas preparative gels for mass spectrometric analysis were stained with colloidal Coomassie. Analytical and preparative gel images stained by silver nitrate or Coomassie blue were digitized using an Imagescanner (GE Healthcare). For each condition, 2 biological and 3 analytical replicates were performed, and only the spots present in all the replicates were taken into consideration for subsequent analysis.

Protein identification by matrix-assisted laser desorption/ionization tandem time-of-flight mass spectrometry (MALDI-TOF/TOF-MS)

Protein identification was performed by peptide mass fingerprinting (PMF) on a 4800 Plus MALDI TOF/TOF instrument

(Applied Biosystems, Foster City, CA, USA). Electrophoretic spots from Coomassie-stained gels were excised and destained in 2.5 mM ammonium bicarbonate and 50% acetonitrile (ACN), and dehydrated in ACN. They were then rehydrated in trypsin solution and digested overnight at 37°C . Each digested (1 μl) protein was spotted onto the MALDI target and allowed to dry. Then 1 μl of matrix solution [saturated solution of α -cyano-4-hydroxycinnamic acid (CHCA) in 50% v/v ACN and 0.1% v/v trifluoroacetic acid (TFA)] was applied to the dried sample, which was dried again. After acquiring the mass of the peptides, a mass fingerprinting search was carried out in the Swiss-Prot/TrEMBL database using Mascot (Matrix Science Ltd., London, UK; <http://www.matrixscience.com>). Taxonomy was limited to *Homo sapiens*, mass tolerance was 40 ppm, and the acceptable number of missed cleavage sites was set at 1. Alkylation of cysteine by carbamidomethylation was assumed, and oxidation of methionine was considered as a possible modification. The criteria used to accept identifications included the extent of sequence coverage ($\geq 10\%$), the number of matched peptides (≥ 4) and a probabilistic score at $P < 0.05$.

Protein identification by LC-MS/MS analysis

Trypsin digests that did not produce unambiguous MALDI-TOF/TOF identifications subsequently underwent peptide sequencing on by nanochip electrospray ionization quantitative TOF (ESI/QTOF) analysis. The mass spectrometer was a 6520 Accurate Mass Q-TOF LC/MS unit (Agilent Technologies, Santa Clara, CA, USA). After injection (3 μl), the peptides were trapped on the enrichment column (4 mm and 40 nl) of a Prot ID-Chip-43(II) (Agilent Technologies) using 100% solvent A (97% HPLC-grade water, 0.1% v/v formic acid, and 3% v/v ACN) at a flow rate of 3 $\mu\text{l}/\text{min}$. After the enrichment phase, separation was performed on the analytical column of the chip (43 mm \times 75 μm) using a linear gradient from 3 to 25% solvent B (5% HPLC-grade water, 95% v/v ACN, and 0.1% v/v formic acid) for 17 min and flow rate of 450 nl/min. A high voltage of 1825 V was applied for stable spray operation. Both MS and MS/MS spectra were acquired using autoMS/MS mode (Agilent MassHunter Workstation acquisition B.02.00). MS spectra were acquired in the 350–1700 *m/z* range, and a maximum of 6 precursors/cycle (2^{+} and 3^{+}) were selected for MS/MS experiments (50–1700 *m/z* range). The MS/MS ion search was carried out in the Swiss-Prot and UniProtKB databases using Mascot. Taxonomy was limited to *Homo sapiens*, peptide precursor charge was set at 2^{+} or 3^{+} , mass tolerance was set at ± 20 ppm for precursor peptide and ± 0.1 Da for fragment peptides, and the acceptable number of missed cleavage sites was set at 1. Alkylation of cysteine by carbamidomethylation was taken as a fixed modification, while oxidation was considered as a possible modification. We considered significant peptides with individual ion scores ($-10 \log [P]$, where P is the probability that the observed match is a random event) that indicated identity ($P < 0.05$).

Functional assays

Apoptosis, mitochondrial O_2^{-} , cellular H_2O_2 , mitochondrial membrane potential (MMP), and mitochondrial mass were measured by flow cytometry. To measure apoptosis, cells were stained with annexin-V Alexa Fluor 488 conjugate in annexin-V binding buffer, to detect phosphatidylserine exposure on the cell surface, and TO-PRO-3 iodide (0.1 μM), to detect loss of plasma membrane integrity (19). When required, mitochondrial O_2^{-} was also measured in live cells as

previously reported (20) by using MitoSOX Red mitochondrial superoxide indicator (Life Technologies). To measure MMP, cells were stained with tetramethylrhodamine, methyl ester (TMRM; Life Technologies) and subjected to flow cytometry. Cellular H_2O_2 was analyzed by staining cells with 2',7'-dichlorodihydrofluorescein diacetate ($H_2DCF-DA$; Life Technologies; ref. 21). In the case of $H_2DCF-DA$ and MitoSOX staining, the mean fluorescence intensity (MFI) of the unstained sample was subtracted from the MFI of the stained sample to avoid any influence related to the eventual autofluorescence. Then, the net MFI value obtained for the control sample was set to 100, and other samples were calculated according the following formula: relative MFI level = (treated sample net MFI/untreated sample net MFI) \times 100. Samples were analyzed using a 16-parameter CyFlow ML flow cytometer (Partec GmbH, Muenster, Germany), equipped with a 488 nm blue solid-state laser, a 635 nm red diode laser, a UV mercury lamp HBO, a 532 nm green solid-state laser, a 405 nm violet laser, and a CCD camera. Data were acquired in list mode by using FloMax (Partec) software and analyzed by FlowJo 9.5.2 (TreeStar) under MacOS X. A minimum of 2×10^4 cells/sample were acquired, and each experiment was repeated ≥ 4 times.

Cellular ATP was measured by Cell Titer-Glo Luminescent Cell Viability Assay (Promega Corp., Madison, WI, USA). Luminescence was measured with an Ascent luminometer (Agilent, Santa Clara, CA, USA). Each experiment was repeated 3 times, and each measurement was performed in duplicate. Data were normalized to protein concentration, which was determined by the Bradford assay.

Total glutathione was measured by Glutathione Assay Kit (Cayman Chemical Co., Ann Arbor, MI, USA), following the manufacturer's instructions. Absorbance was measured with a MR-96A microplate reader (Mindray, Shenzhen, China). Each experiment was repeated ≥ 3 times, and data were normalized according to protein concentration.

Oxygen consumption rate (OCR) in adherent cells was measured with an XF24 Extracellular Flux Analyzer (Seahorse Bioscience, Billerica MA, USA), as described previously (22). Cells (2×10^4 /well) were seeded in XF24 cell culture microplates (Seahorse Bioscience); O_2 calculation method was (LEVEL)Direct (AKOS).

L-lactate in cell culture supernatant was measured by using the L-Lactate Assay Kit I (Eton Biosciences, San Diego, CA, USA). Cells were grown in 12-well plates, and medium concentration was measured by colorimetric assays following the manufacturer's instructions. Absorbance was measured at 490 nm in a MR-96A microplate reader (Mindray). Each experiment was repeated ≥ 3 times. Data are expressed as percentage change with respect to control cells set at 100%.

Statistical analysis

Two-dimensional image analysis was carried out using ImageMaster 2D Platinum 6.0 software (GE Healthcare). Relative spot volumes, calculated as $\%V$ ($V_{\text{single spot}}/V_{\text{total spots}}$ on a gel, where V is the integration of the OD over the spot area), were used for quantitative analyses to decrease experimental errors. The normalized spot volume was averaged, and SD was calculated. A fold change of 2.0 was then chosen as threshold of expression variation. Statistical data were obtained using Prism software (Graph Pad, La Jolla, CA, USA). Protein spot variation was considered significant when showing a P value < 0.05 and \geq a 2-fold change in relative volume $\%V$. For real-time quantitative PCR, and for functional assays, experiments were repeated up to 9 times, significance was determined by Kruskal-Wallis or Mann Whitney tests, and values of $P < 0.05$ were considered significant.

RESULTS

Lon expression is modulated in human cancer cell lines.

In silico analysis of publicly available data has yielded evidence that Lon is often down-regulated in blood tumors (including acute lymphoblastic leukemia, acute myeloid leukemia, and acute promyelocytic leukemia) and up-regulated in many solid tumors, including colon carcinoma (see: <http://www.ebi.ac.uk/gxa/experiment/E-MT-AB-62>). To confirm these data, we monitored Lon expression, both at the mRNA and protein level, in cancer cell lines of different origin in comparison with normal nonproliferating or proliferating cells; relative mRNA and protein levels are reported in **Fig. 1A**. We found that Lon mRNA was expressed at high levels in cells like K562 (human erythromyeloblastoid leukemia), DU145 (prostate carcinoma), PC3 (prostatic adenocarcinoma, grade IV), SHSY5Y (neuroblastoma), MCF7 (breast carcinoma), and RKO (colon carcinoma), if compared to normal resting PBMCs. In particular, Lon relative expression was 0.68 ± 0.38 in resting PBMCs, 1.17 ± 0.33 in PBMCs activated with anti-CD3 plus anti-CD28 monoclonal antibodies, 1.99 ± 1.14 in resting purified B lymphocytes, 2.62 ± 0.48 in CpG DNA-activated B cells, 6.16 ± 3.74 in resting purified monocytes, 4.41 ± 0.25 in lipopolysaccharide-activated monocytes, 30.54 ± 24.93 in K562 cells, 9.46 ± 8.7 in HDLM2, 15.35 ± 14.29 in DU145 cells, 10.19 ± 1.8 in PC3 cells, 14.43 ± 3.8 in RKO cells, 22.79 ± 12.40 in SHSY5Y cells, 7.08 ± 3.9 in HEPG2 cells, and 7.94 ± 0.62 in MCF7 cells. Consistent with mRNA data, Lon protein levels were increased in cell lines from solid tumors, including DU145 cells (3-fold increase), PC3 cells (20-fold increase), RKO cells (15-fold increase), SHSY5Y cells (14-fold increase), and MCF7 cells (10-fold increase), if compared to normal cells (*i.e.*, resting monocytes). Lon protein was indeed expressed at extremely low levels in resting PBMCs from healthy donors, as well as in purified B cells and monocytes, regardless of their activation status.

Lon down-regulation affects cell viability and increases cell susceptibility to apoptosis

We chose the RKO colon cancer cells as a model for evaluating the effects of Lon down-regulation in cells deriving from solid tumors because the quantification of Lon levels in tissue samples from patients with CRC suggested that Lon is up-regulated in cancer cells, compared to the normal mucosal counterparts (**Fig. 1B**). In particular, Lon levels in normal samples were 0.58 ± 0.83 , *vs.* 2.5 ± 1.8 in CRC samples.

First, we ascertained that Lon was actually localized in mitochondria in these cells. By using a custom polyclonal antibody that can identify Lon specifically, we confirmed by immunocytochemical staining that Lon colocalized with mitochondria (**Fig. 1C**). No signal outside mitochondria could be detected.

Then, we targeted Lon mRNA by RNA interference, using

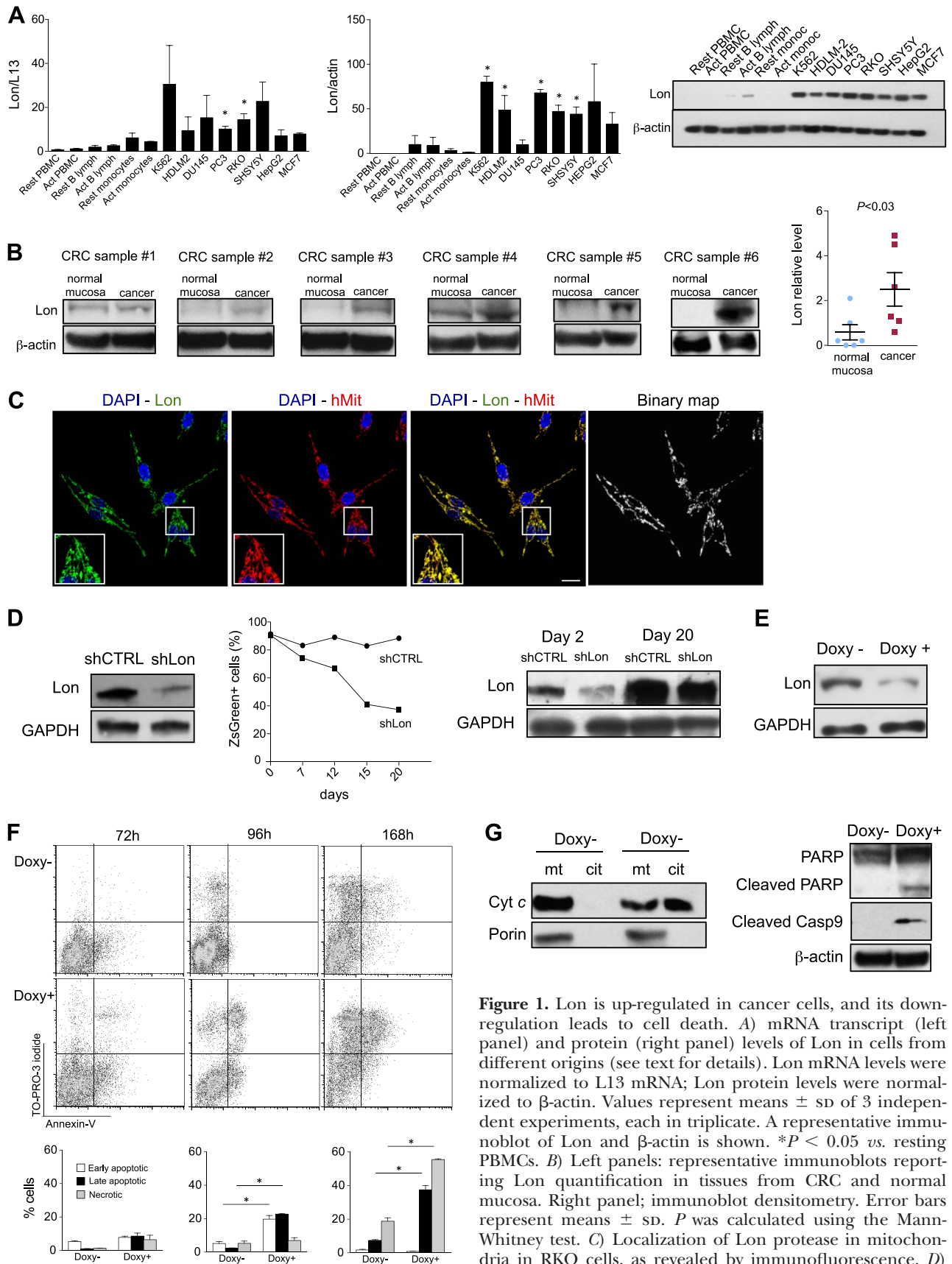


Figure 1. Lon is up-regulated in cancer cells, and its down-regulation leads to cell death. *A*) mRNA transcript (left panel) and protein (right panel) levels of Lon in cells from different origins (see text for details). Lon mRNA levels were normalized to L13 mRNA; Lon protein levels were normalized to β -actin. Values represent means \pm sd of 3 independent experiments, each in triplicate. A representative immunoblot of Lon and β -actin is shown. $*P < 0.05$ vs. resting PBMCs. *B*) Left panels: representative immunoblots reporting Lon quantification in tissues from CRC and normal mucosa. Right panel; immunoblot densitometry. Error bars represent means \pm sd. P was calculated using the Mann-Whitney test. *C*) Localization of Lon protease in mitochondria in RKO cells, as revealed by immunofluorescence. *D*) Immunoblot analysis of Lon from total lysates from cells constitutively expressing an shRNA targeting Lon (shLon) and cells constitutively expressing a scramble shRNA control (shCtrl; left panel); quantification of the percentage of ZsGreen⁺ cells among shCtrl and shLon cells at the indicated time points (middle panel); immunoblot analysis of Lon from total lysates obtained from shLon and shCtrl cells after 2 and 20

(continued on next page)

the retroviral vector RNAi-Ready-pSiren-RetroQ-ZsGreen, which allows a constitutive silencing of the target gene in stably transfected cells. Cells were selected on the basis of ZsGreen expression, and those with the highest ZsGreen fluorescence, that is, those with higher expression of shRNA, were sorted and seeded. As shown in Fig. 1D (left panel), Lon protein was significantly reduced in cells expressing an shRNA targeting Lon (shLon) compared with cells expressing an shRNA control (shCtrl). However, culture of shLon cells for a long time resulted in a progressive decrease of ZsGreen⁺ cells, which represented about 1/3 of cells after 20 d of culture and much less thereafter (not shown); the percentage of ZsGreen⁺ cells remained stable (>95%) in shCtrl (Fig. 1D, middle panel). Indeed, in living ZsGreen⁻ cells a concomitant re-expression of Lon protease, whose levels returned similar to that present in shCtrl, was observed (Fig. 1D, right panel).

Because constitutive down-regulation of Lon resulted in massive cell death, we generated cells where the expression of shLon was inducible by doxy. We obtained a cell clone in which a $71.0 \pm 8.5\%$ reduction of Lon expression was observed after 72 h of treatment with 4 $\mu\text{g}/\text{ml}$ doxy (Fig. 1E). Lon silencing resulted in increased cell death: after 72 h of Lon silencing, early apoptotic cells slightly increased from 5.44 ± 0.89 to 7.8 ± 1.52 , late apoptotic cells from 1.01 ± 0.33 to 8.62 ± 3.59 , and necrotic cells from 1.31 ± 0.27 to 6.49 ± 5.27 . After 96 h, early apoptotic cells increased from 5.99 ± 0.56 to 19.7 ± 3.1 , late apoptotic cells from 2.49 ± 0.04 to 22.8 ± 0.28 , and necrotic cells from 5.28 ± 1.88 to 6.99 ± 2.37 . A more pronounced increase of cell death could be observed after 168 h (Fig. 1F). Then, we analyzed mitochondrial and cytosolic levels of cytochrome *c* (cyt *c*), cleaved caspase-9, and PARP in order to understand if the increased apoptotic cell death is mediated by intrinsic pathway. As shown in Fig. 1G, cells where Lon was down-regulated showed a massive release of cyt *c* in the cytosol (left panel), which led to activation of caspase-9 and PARP (right panel). Thus, silencing of Lon determines apoptosis through cyt *c* release from mitochondria, which led to intrinsic apoptosis.

We decided to perform all the experiments at the conditions of minor cell death, *i.e.*, culturing cells in control medium (doxy⁻), which contains puromycin and G418 but not doxy, and induction medium (doxy⁺), which contains puromycin, G418, and doxy, for 72 h.

Lon down-regulation strongly affects mitochondrial proteome

To identify changes in mitochondrial proteome caused by Lon silencing, we performed 2-DE on proteins isolated

from highly purified mitochondria of RKO cells (Fig. 2A) where Lon was down-regulated. Figure 2B shows a representative image of 2-DE from doxy⁻ and doxy⁺ cells. Sixty-two spots that appeared different in samples from doxy⁻ and doxy⁺ cells were excised from 2-DE gels and submitted for mass spectrometry analysis; 56 were clearly identified as 39 individual proteins. Two spots detected in silver-stained gels were not clearly resolved in preparative gels, and 4 spots, present in very low amounts in analytical gels, were not visible after colloidal Coomassie staining of preparative gels.

The identified spots are listed in Table 1. More than 83.0% of identified proteins were mitochondrial; among them, 26.0% were related to stress response, 14.8% to ribosome assembly, 12.7% to oxidative phosphorylation (oxphos), 8.5% to Krebs cycle, 6.3% to fatty acid β -oxidation, and the remaining 14.7% to mitochondrial crista integrity, ketone body catabolism, mtDNA transcription, and maintenance. If classified on the basis of submitochondrial localization, 29.0% of proteins were identified as matrix proteins, 53% as membrane proteins, and 18.0% as unknown compartment. Seventeen protein spots, which correspond to 9 individual proteins, namely ATP5J, ATPA, CH60, GRP75, HSPB1, PDIA3, S10AB, UCRI, and VDACL1, were more abundant in mitochondria from Lon-deficient cells. Conversely, 39 protein spots, which correspond to 24 individual proteins, were decreased in mitochondria from Lon-deficient cells (Fig. 2C).

To further confirm these results, we selected 4 representative proteins (EFTu, UCRI, GRP75, and MDHM) and reanalyzed their expression in the same cells by Western blot. As expected, Lon down-regulation caused an increase of GRP75 and a reduction of EFTu, UCRI, and MDHM (Fig. 2D, E). Finally, we monitored the expression levels of selected possible Lon targets in cells in which Lon was not silenced. For this, we treated RKO cultures with CDDO, a triterpenoid able to inhibit Lon proteolytic activity in a dose-dependent manner (23). Cells were treated with 0.1 and 1 μM CDDO, and the expression of the aforementioned representative proteins was assessed. Similar to what was observed after Lon silencing, CDDO modulated their expression in a dose-dependent manner (Fig. 2F).

Lon down-regulation impairs mitochondrial function

Because Lon is deeply involved in mtDNA maintenance, mainly through the regulation of TFAM (24), we measured the levels of mtDNA, mtRNAs, and TFAM in control and silenced cells. While mtDNA levels were almost unchanged (Fig. 3A), mitochondrial transcripts

d of culture (right panel). E) Immunoblot analysis of RKO cells where Lon was down-regulated by doxy. F) Cytofluorimetric quantification of early and late apoptotic cells and of necrotic cells after 72, 96, and 168 h of culture in RKO cells where Lon was down-regulated by doxy. Representative dot plots reporting annexin-V staining *vs.* TO-PRO-3 iodide staining are reported, together with the quantification of apoptotic cells obtained from 45 independent experiments; data represent means \pm sd. * $P < 0.05$. G) Left panel: immunoblot analysis of cytochrome *c* (cyt *c*) in mitochondrial fraction obtained from RKO cells where Lon was down-regulated by doxy. Right panel: immunoblot analysis of PARP and cleaved caspase 9 in total lysates from RKO cells where Lon was down-regulated by doxy.

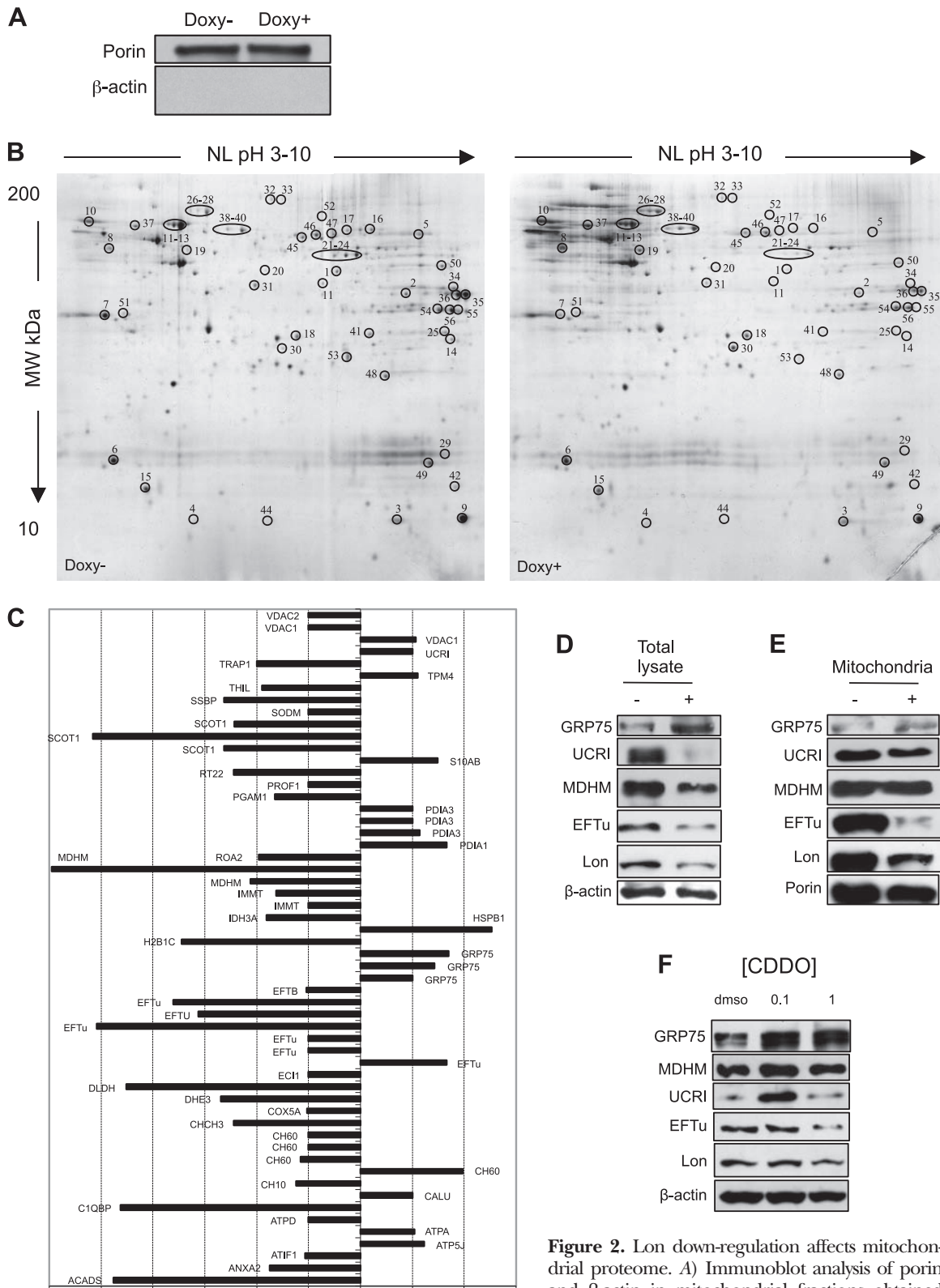


Figure 2. Lon down-regulation affects mitochondrial proteome. *A*) Immunoblot analysis of porin and β -actin in mitochondrial fractions obtained from doxy⁻ and doxy⁺ cells. *B*) Representative 2-DE images of mitochondrial proteins were obtained from doxy-regulated RKO cells. Numbers indicate spots that are significantly different between doxy⁻ and doxy⁺ cells ($P < 0.05$; Student's *t* test). *C*) Quantitative analysis of spots identified by mass spectrometry. Spot quantification (percentage volume of each spot) was performed on 2-DE using ImageMaster 2D Platinum 6.0 software. *D*) Immunoblot analysis of total lysates from doxy⁻ (-) and doxy⁺ (+) cells for the following proteins: GRP75, UCRI, MDHM, EFTu, Lon, and β -actin. *E*) Immunoblot analysis of mitochondrial fractions from doxy⁻ (-) and doxy⁺ (+) cells for the following proteins: GRP75, UCRI, MDHM, EFTu, Lon, and porin. *F*) Immunoblot analysis of total lysates from RKO cells treated with CDDO (0.1 to 1 μ M) for the following proteins: GRP75, MDHM, UCRI, EFTu, Lon, and β -actin.

TABLE 1. Qualitative and quantitative data and associated statistics from 2-DE analysis

Short name	Protein name	UniProt ID	Matched/ searched sequences	Score	Sequence coverage (%)	Theoretical MW (Da)
ACADS	Short-chain specific acyl-CoA dehydrogenase	P16219	12/14	535	40	44,611
ANXA2	Annexin A2	P07355	4/6	98	24	38,808
ATIF1	ATPase inhibitor	Q9UII2	4/4	184	16	12,241
ATP5J	ATP synthase-coupling factor 6	P18859	7/7	671	53	12,580
ATPA	ATP synthase subunit α	P25705	20/36	1664	67	59,828
ATPD	ATP synthase subunit δ	P30049	6/8	946	46	17,479
CIQBP	Complement component 1 Q subcomponent-binding protein	Q07021	5/5	132	41	31,742
CALU	Calumenin	O43852	17/24	836	72	37,198
CH10	10 kDa heat shock protein	P61604	7/8	356	54	10,925
CH-60	60 kDa heat shock protein	P10809	12/24	1339	47	61,187
CH-60	60 kDa heat shock protein	P10809	11/14	499	28	61,187
CH-60	60 kDa heat shock protein	P10809	11/11	796	25	61,187
CH-60	60 kDa heat shock protein	P10809	14/16	829	33	61,187
CHCH3	Coiled-coil-helix-coiled-coil-helix domain-containing protein 3	Q9NX63	16/19	837	52	26,421
COX5A	Cytochrome c oxidase subunit 5A	P20674	9/9	882	38	16,923
DHE3	Glutamate dehydrogenase 1	P00367	10/14	334	26	61,701
DLDH	Dihydrolipoyl dehydrogenase	P09622	20/25	1126	56	54,713
ECI1	Enoyl-CoA δ isomerase 1	P42126	13/13	1080	56	33,080
EFTU	Elongation factor Tu	P49411	8/23	623	55	49,852
EFTU	Elongation factor Tu	P49411	4/13	160	32	49,852
EFTU	Elongation factor Tu	P49411	11/11	533	31	49,852
EFTU	Elongation factor Tu	P49411	12/12	767	33	49,852
EFTU	Elongation factor Tu	P49411	15/15	591	43	49,852
EFTU	Elongation factor Tu	P49411	28/33	3646	77	49,852
ETFB	Electron transfer flavoprotein subunit beta	P38117	18/19	987	65	28,054
GRP75	Stress-70 protein, mitochondrial	P38646	15/16	848	28	73,920
GRP75	Stress-70 protein, mitochondrial	P38646	14/15	862	26	73,920
GRP75	Stress-70 protein, mitochondrial	P38646	10/10	510	19	73,920
H2B1C	Histone H2B type 1-C/E/F/G/I	P62807	5/12	616	63	13,898
HSPB1	Heat shock protein β -1	P04792	4/5	80	29	22,826
IDH3A	Isocitrate dehydrogenase [NAD] subunit alpha	P50213	5/7	217	22	40,022
IMMT	Mitochondrial inner membrane protein	Q16891	24/50	1029	55	84,026
IMMT	Mitochondrial inner membrane protein	Q16891	29/51	1376	50	84,026
MDHM	Malate dehydrogenase	P40926	13/14	477	45	35,937
MDHM	Malate dehydrogenase	P40926	17/21	1709	67	35,937
PDIA1	Protein disulfide-isomerase	P07237	29/47	2073	80	57,480
PDIA3	Protein disulfide-isomerase A3	P30101	25/35	1413	61	57,146
PDIA3	Protein disulfide-isomerase A3	P30101	28/41	3061	65	57,146
PDIA3	Protein disulfide-isomerase A3	P30101	13/13	522	28	57,146
PGAM1	Phosphoglycerate mutase 1	P18669	10/18	355	77	28,900
PROF1	Profilin-1	P07737	9/13	866	75	15,216
ROA2	Heterogeneous nuclear ribonucleoproteins A2/B1	P22626	5/7	144	22	37,464
RT22	28S ribosomal protein S22	P82650	7/8	281	27	41,425
S10AB	Protein S100-A11	P31949	4/5	193	49	11,847
SCOT1	Succinyl-CoA:3-ketoacid coenzyme A transferase 1	P55809	19/25	1088	64	56,578
SCOT1	Succinyl-CoA:3-ketoacid coenzyme A transferase 1	P55809	5/5	160	15	56,578
SCOT1	Succinyl-CoA:3-ketoacid coenzyme A transferase 1	P55809	10/10	425	27	56,578
SODM	Superoxide dismutase [Mn]	P04179	7/8	316	27	24,878
SSBP	Single-stranded DNA-binding protein	Q04837	5/7	200	40	17,249
THIL	Acetyl-CoA acetyltransferase	P24752	12/33	820	83	45,456
TPM3	Tropomyosin α -3 chain	P06753	10/17	198	40	32,856
TRAP1	Heat shock protein 75 kDa	Q12931	21/46	857	68	80,345
UCRI	Cytochrome b-c1 complex subunit Rieske	P47985	8/10	579	34	29,934
VDAC1	Voltage-dependent anion-selective channel protein 1	P21796	9/9	271	46	30,868
VDAC1	Voltage-dependent anion-selective channel protein 1	P21796	15/23	2014	77	30,868
VDAC2	Voltage-dependent anion-selective channel protein 2	P45880	12/16	1601	65	32,060

Differentially expressed protein spots identified by mass spectrometry. UniProt ID indicates Swiss-Prot/TrEMBL accession number. Score indicates percentage of amino acid sequence coverage of matched peptides in the identified proteins. Sequence coverage indicates Mascot score (Matrix Science; <http://www.matrixscience.com>).

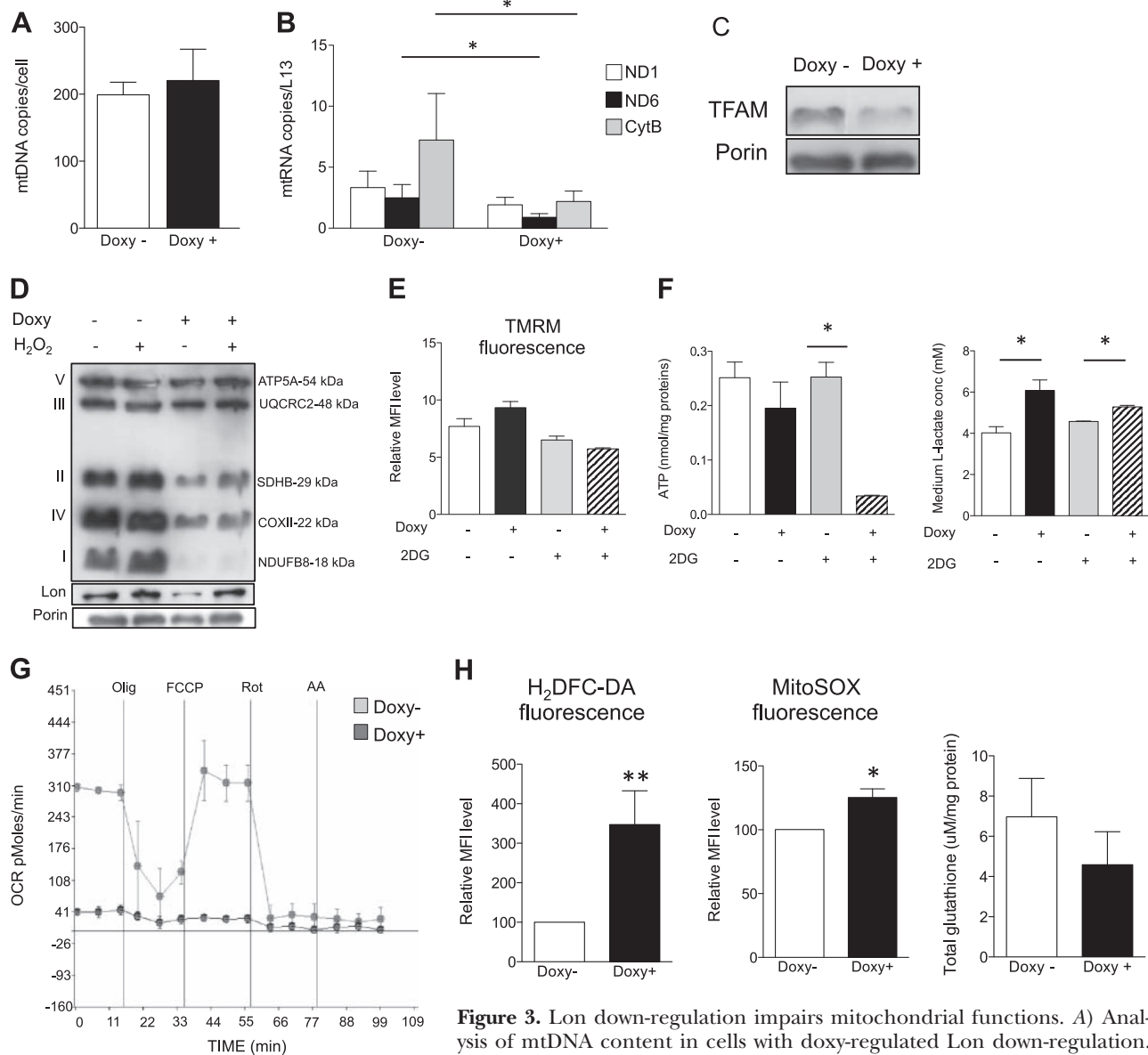


Figure 3. Lon down-regulation impairs mitochondrial functions. *A*) Analysis of mtDNA content in cells with doxy-regulated Lon down-regulation. Values represent means \pm SD of 6 independent experiments, each in triplicate. $*P < 0.05$. *C*) Immunoblot analysis of TFAM protein levels. *D*) Immunoblot analysis of electron transport chain proteins in cells with doxy-regulated Lon decrease, both at the steady-state level and in the presence of H_2O_2 . *E*) Analysis of MMP in cells with doxy-regulated Lon silencing, and in the presence of 80 mM for 2 h. MMP was analyzed by flow cytometry by using TMRM. *F*) Left panel: quantification of ATP levels in cells with doxy-regulated Lon silencing, and in the presence of 80 mM for 2 h. Right panel: quantification of L-lactate concentration in medium of cells with doxy-regulated Lon silencing, and in the presence of 80 mM for 2 h. Values represent means \pm SD of 9 independent experiments. $*P < 0.05$. *G*) Representative traces of OCR experiments performed on monolayers of viable RKO cells. Vertical lines indicate progressive additions of ATP synthase inhibitor oligomycin (Olig, 1 μ M), carbonyl cyanide-4-(trifluoromethoxy)phenylhydrazone (FCCP; 0.2 μ M in doxy⁻ cells and 0.4 μ M in doxy⁺ cells), rotenone (Rot, 1 μ M), and antimycin A (AA, 1 μ M), respectively. *H*) Left panel: detection of hydrogen peroxide in cells with doxy-regulated Lon expression, as revealed by flow cytometry by using H_2DCF -DA probe. Values represent mean \pm SD percentage of increase in MFI of 4 independent experiments. Middle panel: detection of mitochondrial anion superoxide in cells with doxy-regulated Lon expression, as revealed by flow cytometry by using MitoSOX probe. Values represent mean \pm SD percentage of increase in MFI of 4 independent experiments. Right panel: detection of total glutathione (GSH) in cells with doxy-regulated Lon expression; values represent means \pm SD of 6 independent experiments. $*P < 0.05$, $**P < 0.01$.

for ND1, ND6, and cytB in doxy⁺ cells showed a 57.0, 35.7, and 29.9% reduction, respectively (Fig. 3B). We also observed a concomitant reduction of TFAM protein ($51.0 \pm 4.8\%$), the main factor driving mtDNA transcription (Fig. 3C).

As levels of mtRNAs encoding components of the respiratory chain appeared severely reduced, we analyzed the steady-state levels of oxphos complex by using 5 mAbs, one each against complex I subunit NDUFB8, complex II subunit 30 kDa (30 kDa IP), complex III

subunit core 2 (core 2), complex IV subunit II (COXII), and ATP synthase subunit α (F₁a). The 30 kDa IP, COXII, and NDUFB8 were markedly reduced (Fig. 3D), meaning that complex I, complex II, and complex IV were severely affected by Lon down-regulation; complex I was the most altered, with a >90% reduction in silenced cells. Complex II and complex IV had a 70 and 61% decrease, respectively. Treatment with H₂O₂ increased Lon level, as expected; such increase was also observed in doxy⁺ cells, where up-regulation of Lon by H₂O₂ counteracted, even if not completely, silencing by shRNA. However, the partial recovery of Lon induced by H₂O₂ was not sufficient to reestablish the normal levels of oxphos proteins (Fig. 3D). Mitochondrial membrane potential, as assayed by TMRM, was not altered by Lon silencing (Fig. 3E).

Next, we asked whether these changes significantly alter mitochondrial functionality, by evaluating ATP basal levels and the OCR in control and silenced cells. Down-regulation of Lon caused a reduction of ATP levels, which dropped from 0.25 ± 0.04 to 0.03 ± 0.001 nmol/mg proteins in the presence of 2DG (Fig. 3F, left panel). A parallel 1.5-fold increase of L-lactate concentration in culture medium was also observed (Fig. 3F, right panel). Furthermore, Lon silencing caused a marked decrease in mitochondrial respiration, and abolished both basal and carbonyl cyanide-4-(trifluoromethoxy)phenylhydrazone (FCCP)-stimulated OCR (Fig. 3G).

To evaluate the redox status of Lon-deficient cells, reactive oxygen species and total glutathione were measured. We observed a 3-fold increase of relative levels of H₂O₂ in cells where Lon was down-regulated (Fig. 3H, left panel). A 1.3-fold increase of mtO₂⁻ can be also observed (Fig. 3H, middle panel); these changes were accompanied by a 1.5-fold reduction in the level of total glutathione (Fig. 3H, right panel).

Lon down-regulation alters mitochondrial morphology

We wondered whether impaired electron transport chain resulted in alterations of mitochondria morphology. As reported in Fig. 4A, B, silenced cells were characterized by an increase in the number of dying cells, some exhibiting superficial blebs, a typical sign of apoptosis. Control cells showed typical elongated mitochondria characterized by cristae running parallel one to the other within an electron-dense matrix (Fig. 4C, E). By contrast, in Lon-deficient cells, numerous mitochondria were very heterogeneous in size and shape (Fig. 4D, F) and were characterized by dilated cristae, vacuoles, and heavily electron-dense deforming inclusions (Fig. 4G, H). The variety of mitochondrial morphological alterations might reflect the extent of impaired oxphos function and perhaps a different response of the cells depending on their metabolism. Several cells also showed autophagic vacuoles (Fig. 5A). Consistently, the amount of LC3-II, which is a marker of autophagy, increased in silenced cells (Fig. 5B).

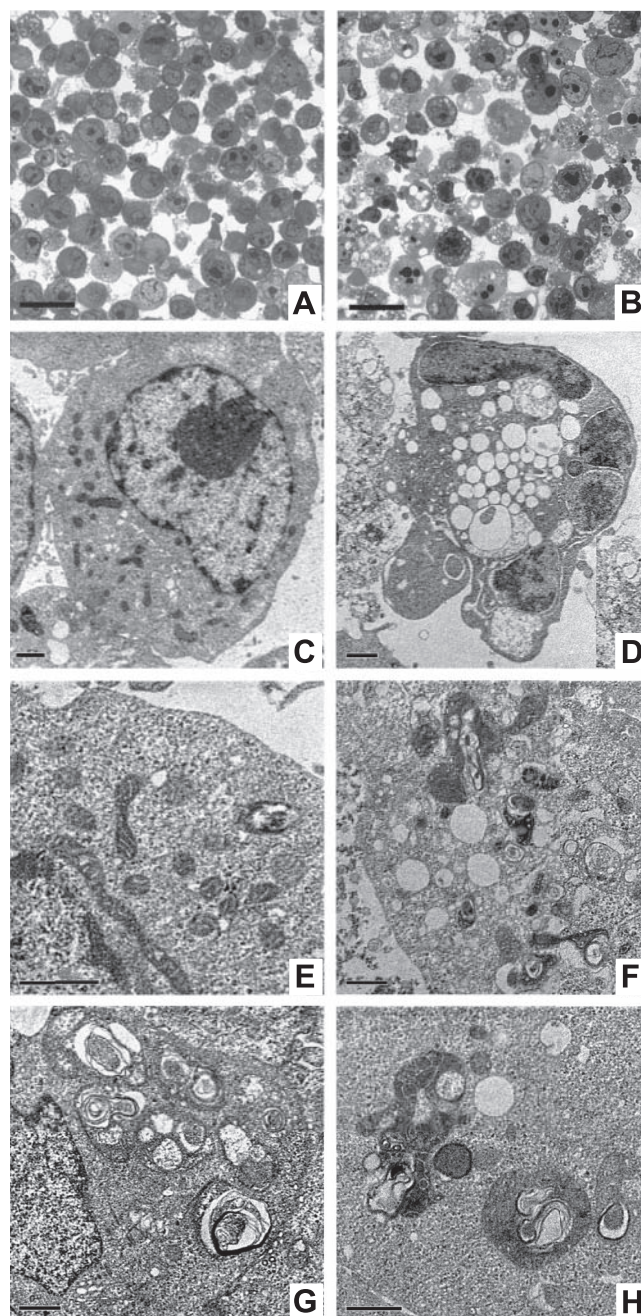


Figure 4. Lon down-regulation affects mitochondrial architecture. Representative images obtained by transmission electron microscopy of doxy⁻ (A, C, E) and doxy⁺ (B, D, F–H) cells. Scale bars = 1 μ m.

Confocal microscopy further confirmed this observation and revealed a different shape of mitochondrial network in Lon-silenced cells and control cells (Fig. 5C and Supplemental Videos S1 and S2). These changes did not affect the total number of mitochondria, as well as the mitochondrial network volume (Fig. 5D), which were similar in silenced and control cells; the mean volume of a single mitochondrion was increased 1.5-fold (Fig. 5D, middle panel). Alteration of mitochondrial architecture was also consistent with down-regulation of IMMT and CHCH3, observed in proteomic analysis.

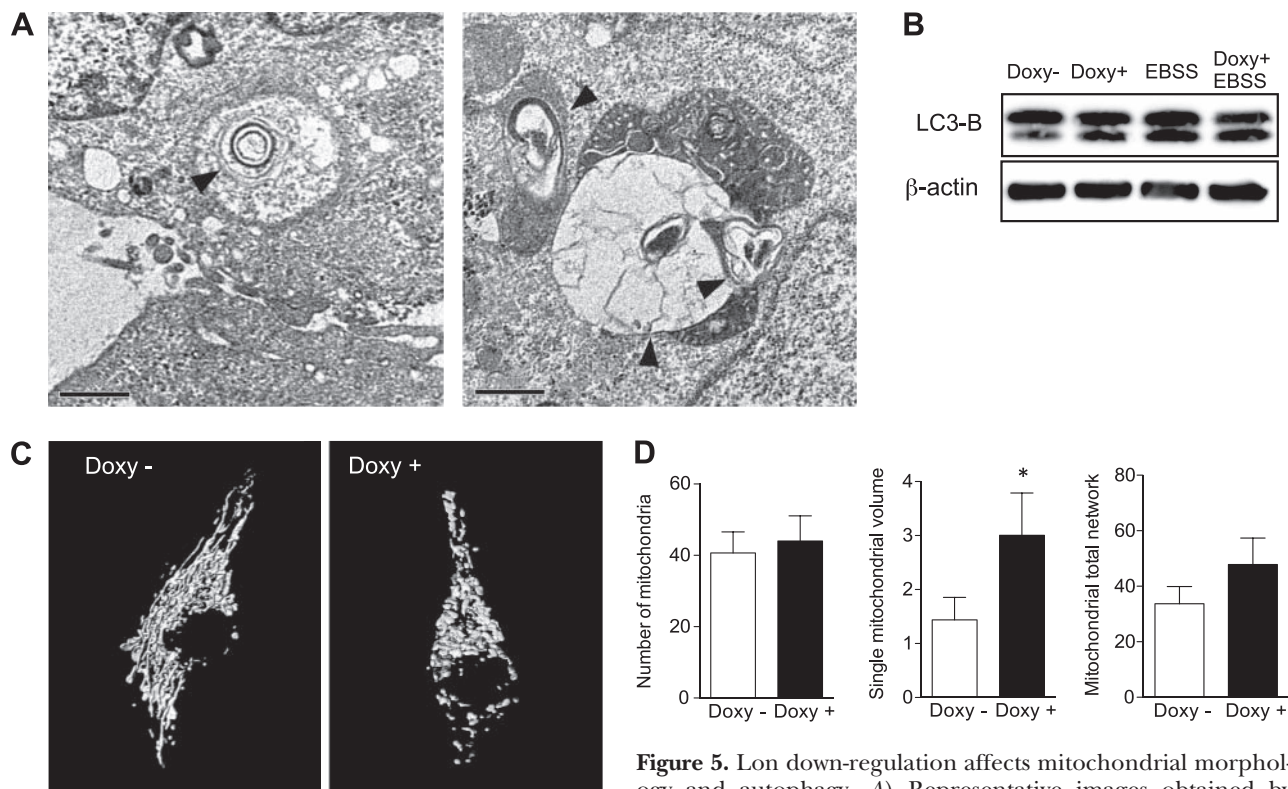


Figure 5. Lon down-regulation affects mitochondrial morphology and autophagy. *A*) Representative images obtained by electron microscopy of RKO cells, showing a typical example of autophagy (left panel) and mitophagy (right panel) as they are frequently observed in silenced cells. Arrowheads indicate double membranes. Scale bars = 1 μ m. *B*) Immunoblot analysis of LC3-B, as marker of autophagy, in lysates from doxy-regulated RKO cells, both at the steady-state level and in the presence of Earle's balanced salt solution (EBSS). *C*) Representative 3-D confocal microscopy images of mtDsRed-labeled mitochondria in control and silenced cells (see Supplemental Videos S1 and S2). *D*) Quantitative analysis of changes in mitochondrial morphology: total number of mitochondria (left panel), single mitochondrial volume (middle panel), and mitochondrial network (right panel). Values represent means \pm sd of 20 independent quantifications. * $P < 0.05$.

autophagy (left panel) and mitophagy (right panel) as they are frequently observed in silenced cells. Arrowheads indicate double membranes. Scale bars = 1 μ m. *B*) Immunoblot analysis of LC3-B, as marker of autophagy, in lysates from doxy-regulated RKO cells, both at the steady-state level and in the presence of Earle's balanced salt solution (EBSS). *C*) Representative 3-D confocal microscopy images of mtDsRed-labeled mitochondria in control and silenced cells (see Supplemental Videos S1 and S2). *D*) Quantitative analysis of changes in mitochondrial morphology: total number of mitochondria (left panel), single mitochondrial volume (middle panel), and mitochondrial network (right panel). Values represent means \pm sd of 20 independent quantifications. * $P < 0.05$.

DISCUSSION

We have found that mitochondrial Lon protease, which is expressed at high levels in several tumors but not in normal or highly proliferating, nontransformed cells, is essential for maintaining the functionality and morphology of mitochondria in RKO colon carcinoma cancer cells, as well as for their survival.

Although the role of Lon in the control of mitochondrial protein quality has been described in bacteria and in yeast (25), the effects of its silencing are scarcely known in human cells. We found that in RKO cells, the down-regulation of Lon deeply affects mitochondrial proteome, causing significant changes (either increase or decrease) of proteins involved in stress response, respiratory chain assembly, energetic metabolism, and ribosome assembly. Such complex changes can be explained considering the dual function of Lon, which acts as a protease and as a chaperone (12). Indeed, Lon removes damaged enzymes from the organelle but also supports the folding and assembly of the matrix and inner membrane respiratory chain complexes (for the subunits encoded by mtDNA as well as for those encoded by nuclear DNA and imported into mitochondria).

The marked reduction of some electron transport chain subunits, such as NDUFB8, COXII, and SDHB, is probably due to their misfolding. Conversely, the increased levels of proteins like UCRI, ATPA, and ATP5J, among others, indicate that such proteins could be possible targets of Lon proteolytic activity. The up-regulation of GRP75 and PDIA3, two proteins associated with the response to protein misfolding and aggregation, supports this observation. In addition, PDIA3 catalyzes isomerization, reduction, and oxidation of disulfides and provides a link between protein misfolding and apoptotic cell death (26). The changes in mitochondrial proteome of Lon-silenced cells were due to proteolytic activity of Lon, since the treatment of cells with CDDO, an inhibitor of Lon proteolytic activity, had the same effect of gene silencing.

Alterations in mitochondrial proteome in Lon-silenced cells showed a certain degree of overlap with those observed in *Saccharomyces cerevisiae* knocked down for Pim1/Lon (27, 28). Overlapping proteins included mitochondrial superoxide dismutase, mitochondrial heat shock protein 70 chaperone, mitochondrial heat shock protein 60, isocitrate dehydrogenase subunit 2, dihydrolipoyl dehydrogenase, malate dehydrogenase, voltage-dependent anion-selective channel protein 2,

and some subunits of ATP synthase, further highlighting the crucial importance of Lon, and its conservation throughout evolution. However, significant discrepancies in the mitochondrial proteome between humans and yeast exist, probably because some of the substrates of Pim1 observed in yeast have no counterpart in human mitochondria. Nevertheless, in both cases Lon/Pim1 appears crucial for the correct assembly of inner membrane complexes (in particular ATP synthase), and in both cases the main functional consequence of Lon/Pim1 absence in the cell is the same; *i.e.*, the almost complete loss of respiration capability. Direct analysis of Lon proteolytic activity of human proteins identified as putative substrates will shed light on the role of this protease in the normal turnover of mitochondrial proteome.

The marked changes of mitochondrial proteome we observed have a deep effect on mitochondrial functionality and morphology. First, we observed significant changes in the expression of mtRNAs. This finding highlights the crucial role of Lon for the expression of oxphos subunit deriving from mtDNA, and for the stability of the transcription machinery. In yeast, the deletion of Pim1 results in large mtDNA mutations that severely affect mitochondria-encoded subunits of respiratory complexes or mitochondrial ribosomes (29). The lack of significant changes in mtDNA content, which has been measured in Lon-silenced cells after 72 h of culture, can be explained taking into account the short period of culture, when a reasonable number of viable cells is likely still present. Current studies aim to detect the presence of possible mtDNA mutations. As such, the reduction that we observed of EFTu and RT22, two proteins involved in ribosome assembly, could explain the decrease of oxphos polypeptides, at least for those encoded by mtDNA. Second, along with alterations in mitochondrial transcripts levels, Lon silencing causes a reduction of several subunits of mitochondrial inner membrane complexes, with Complex I the most affected. A link between Lon and complex I has also been reported (30). These alterations have a dramatic effect on cellular respiratory capacity, which is severely impaired in the basal conditions and did not increase, even in the presence of FCCP. Similarly, impairment in OCR and in extracellular acidification rate has been observed in HeLa cells where Lon was down-regulated by shRNA (31).

Third, we saw that mitochondrial architecture and morphology was profoundly altered. The presence of electron-dense inclusion bodies inside mitochondria confirms that unfolded proteins accumulate when Lon is down-regulated. Moreover, the down-regulation of IMMT and CHCH3, which belong to the MINOS complex and are crucial organizers of mitochondrial architecture, can explain changes in shape and volume of mitochondria.

The presence of higher levels of autophagy is likely not sufficient to eliminate these damaged mitochondria; indeed, apoptosis is highly present among such cells. While it is evident that Lon down-regulation leads

to apoptosis through cyt *c* release and activation of intrinsic pathway, Lon probably has an indirect, rather than direct, role in inducing apoptosis. Indeed, many of the proteins involved in the regulation of apoptotic cell death are located between the inner and outer mitochondrial membranes and thus inaccessible to Lon. Moreover, no direct interaction among Lon and proteins related to the regulation of apoptosis (including proteins such as AIF) has been revealed by proteomic analysis. Conversely, the presence of inclusion bodies, the loss of cristae and the deep alteration of mitochondrial morphology—without loss of MMP—strongly suggest that apoptosis is a secondary consequence of the altered mitochondrial architecture, which in turn determines loss of mt membrane integrity and leak of cyt *c*.

In our model, we could never obtain a 100% depletion of Lon. This result is in fact normal when shRNAs are used for knocking down genes. Nevertheless, it must be noted that a down-regulation of ~90% can still cause dramatic alterations of mitochondrial morphology and functionality; this observation suggests that Lon expression must be maintained above a threshold value, in order to guarantee a full functionality of the organelle. The fact that the down-regulation of Lon, or even its inhibition, might cause the death of colon cancer cells can pave new ways for controlling tumors, likely through the identification of molecules or strategies able to inhibit Lon activity. EJ

This work was supported by grants from Associazione Italiana Ricerca sul Cancro (grant 11341 to A.C.), Ministero Istruzione, Università, Ricerca (grant RBAP11S8C3 to A.C. and P.B.), and Fondazione Cassa di Risparmio di Vignola (grant to M.P.).

REFERENCES

1. Markowitz, S. D., and Bertagnolli, M. M. (2009) Molecular origins of cancer: molecular basis of colorectal cancer *N. Engl. J. Med.* **361**, 2449–2460
2. Chiacchiera, F., Matrone, A., Ferrari, E., Ingravallo, G., Lo Sasso, G., Murzilli, S., Petruzzelli, M., Salvatore, L., Moschetta, A., and Simone, C. (2009) p38alpha blockade inhibits colorectal cancer growth in vivo by inducing a switch from HIF1alpha- to FoxO-dependent transcription. *Cell Death Differ.* **16**, 1203–1214
3. Huang, C. Y., Kuo, W. T., Huang, Y. C., Lee, T. C., and Yu, L. C. (2013) Resistance to hypoxia-induced necroptosis is conferred by glycolytic pyruvate scavenging of mitochondrial superoxide in colorectal cancer cells. *Cell Death Dis.* **4**, e622
4. Rasheed, S., Harris, A. L., Tekkis, P. P., Turley, H., Silver, A., McDonald, P. J., Talbot, I. C., Glynne-Jones, R., Northover, J. M., and Guenther, T. (2009) Hypoxia-inducible factor-1alpha and -2alpha are expressed in most rectal cancers but only hypoxia-inducible factor-1alpha is associated with prognosis. *Br. J. Cancer* **100**, 1666–1673
5. Xu, J., Wang, J., Xu, B., Ge, H., Zhou, X., and Fang, J. Y. (2013) Colorectal cancer cells refractory to anti-VEGF treatment are vulnerable to glycolytic blockade due to persistent impairment of mitochondria. *Mol. Cancer Ther.* **12**, 717–724
6. Weinberg, F., Hamanaka, R., Wheaton, W. W., Weinberg, S., Joseph, J., Lopez, M., Kalyanaraman, B., Mutlu, G. M., Budinger, G. R., and Chandel, N. S. (2010) Mitochondrial metabolism and ROS generation are essential for Kras-mediated tumorigenicity. *Proc. Natl. Acad. Sci. U. S. A.* **107**, 8788–8793

7. Suzuki, C. K., Suda, K., Wang, N., and Schatz, G. (1994) Requirement for the yeast gene LON in intramitochondrial proteolysis and maintenance of respiration. *Science* **264**, 273–276
8. Bayot, A., Gareil, M., Rogowska-Wrzesinska, A., Roepstorff, P., Friguet, B., and Bulteau, A. L. (2010) Identification of novel oxidized protein substrates and physiological partners of the mitochondrial ATP-dependent Lon-like protease Pim1. *J. Biol. Chem.* **285**, 11445–11457
9. Friguet, B., Bulteau, A. L., and Petropoulos, I. (2008) Mitochondrial protein quality control: implications in ageing. *Biotechnol. J.* **3**, 757–764
10. Chen, S. H., Suzuki, C. K., and Wu, S. H. (2008) Thermodynamic characterization of specific interactions between the human Lon protease and G-quartet DNA. *Nucleic Acids Res.* **36**, 1273–1287
11. Lu, B., Yadav, S., Shah, P. G., Liu, T., Tian, B., Puksza, S., Villaluna, N., Kutejova, E., Newlon, C. S., Santos, J. H., and Suzuki, C. K. (2007) Roles for the human ATP-dependent Lon protease in mitochondrial DNA maintenance. *J. Biol. Chem.* **282**, 17363–17374
12. Hori, O., Ichinoda, F., Tamatani, T., Yamaguchi, A., Sato, N., Ozawa, K., Kitao, Y., Miyazaki, M., Harding, H. P., Ron, D., Tohyama, M., D. M. S., and Ogawa, S. (2002) Transmission of cell stress from endoplasmic reticulum to mitochondria: enhanced expression of Lon protease. *J. Cell Biol.* **157**, 1151–1160
13. Ngo, J. K., and Davies, K. J. (2009) Mitochondrial Lon protease is a human stress protein. *Free Radic. Biol. Med.* **46**, 1042–1048
14. Goard, C. A., and Schimmer, A. D. (2013) Mitochondrial matrix proteases as novel therapeutic targets in malignancy. *Oncogene* **33**, 2690–2699
15. Luce, K., Weil, A. C., and Osiewacz, H. D. (2010) Mitochondrial protein quality control systems in aging and disease. *Adv. Exp. Med. Biol.* **694**, 108–125
16. Pinti, M., Gibellini, L., Guaraldi, G., Orlando, G., Gant, T. W., Morselli, E., Nasi, M., Salomoni, P., Mussini, C., and Cossarizza, A. (2010) Upregulation of nuclear-encoded mitochondrial LON protease in HAART-treated HIV-positive patients with lipodystrophy: implications for the pathogenesis of the disease. *AIDS* **24**, 841–850
17. Addis, M. F., Tanca, A., Pagnozzi, D., Crobu, S., Fanciulli, G., Cossu-Rocca, P., and Uzzau, S. (2009) Generation of high-quality protein extracts from formalin-fixed, paraffin-embedded tissues. *Proteomics* **9**, 3815–3823
18. Cossarizza, A., Riva, A., Pinti, M., Ammannato, S., Fedeli, P., Mussini, C., Esposito, R., and Galli, M. (2003) Increased mitochondrial DNA content in peripheral blood lymphocytes from HIV-infected patients with lipodystrophy. *Antivir. Ther.* **8**, 315–321
19. Troiano, L., Ferraresi, R., Lugli, E., Nemes, E., Roat, E., Nasi, M., Pinti, M., and Cossarizza, A. (2007) Multiparametric analysis of cells with different mitochondrial membrane potential during apoptosis by polychromatic flow cytometry. *Nat. Protoc.* **2**, 2719–2727
20. Mukhopadhyay, P., Rajesh, M., Hasko, G., Hawkins, B. J., Madesh, M., and Pacher, P. (2007) Simultaneous detection of apoptosis and mitochondrial superoxide production in live cells by flow cytometry and confocal microscopy. *Nat. Protoc.* **2**, 2295–2301
21. Cossarizza, A., Ferraresi, R., Troiano, L., Roat, E., Gibellini, L., Bertoncelli, L., Nasi, M., and Pinti, M. (2009) Simultaneous analysis of reactive oxygen species and reduced glutathione content in living cells by polychromatic flow cytometry. *Nat. Protoc.* **4**, 1790–1797
22. Giorgio, V., Petronilli, V., Ghelli, A., Carelli, V., Rugolo, M., Lenaz, G., and Bernardi, P. (2012) The effects of idebenone on mitochondrial bioenergetics. *Biochim. Biophys. Acta* **1817**, 363–369
23. Bernstein, S. H., Venkatesh, S., Li, M., Lee, J., Lu, B., Hilchey, S. P., Morse, K. M., Metcalfe, H. M., Skalska, J., Andreeff, M., Brookes, P. S., and Suzuki, C. K. (2012) The mitochondrial ATP-dependent Lon protease: a novel target in lymphoma death mediated by the synthetic triterpenoid CDDO and its derivatives. *Blood* **119**, 3321–3329
24. Lu, B., Lee, J., Nie, X., Li, M., Morozov, Y. I., Venkatesh, S., Bogenhagen, D. F., Temiakov, D., and Suzuki, C. K. (2013) Phosphorylation of human TFAM in mitochondria impairs DNA binding and promotes degradation by the AAA+ Lon protease. *Mol. Cell* **49**, 121–132
25. Bender, T., Leidhold, C., Ruppert, T., Franken, S., and Voos, W. (2010) The role of protein quality control in mitochondrial protein homeostasis under oxidative stress. *Proteomics* **10**, 1426–1443
26. Hoffstrom, B. G., Kaplan, A., Letso, R., Schmid, R. S., Turmel, G. J., Lo, D. C., and Stockwell, B. R. (2010) Inhibitors of protein disulfide isomerase suppress apoptosis induced by misfolded proteins. *Nat. Chem. Biol.* **6**, 900–906
27. Major, T., von Janowsky, B., Ruppert, T., Mogk, A., and Voos, W. (2006) Proteomic analysis of mitochondrial protein turnover: identification of novel substrate proteins of the matrix protease pim1. *Mol. Cell. Biol.* **26**, 762–776
28. Von Janowsky, B., Knapp, K., Major, T., Krayl, M., Guiard, B., and Voos, W. (2005) Structural properties of substrate proteins determine their proteolysis by the mitochondrial AAA+ protease Pim1. *Biol. Chem.* **386**, 1307–1317
29. Van Dyck, L., Pearce, D. A., and Sherman, F. (1994) PIM1 encodes a mitochondrial ATP-dependent protease that is required for mitochondrial function in the yeast *Saccharomyces cerevisiae*. *J. Biol. Chem.* **269**, 238–242
30. Cheng, C. W., Kuo, C. Y., Fan, C. C., Fang, W. C., Jiang, S. S., Lo, Y. K., Wang, T. Y., Kao, M. C., and Lee, A. L. (2013) Overexpression of Lon contributes to survival and aggressive phenotype of cancer cells through mitochondrial complex I-mediated generation of reactive oxygen species. *Cell Death Dis.* **4**, e681
31. Nie, X., Li, M., Lu, B., Zhang, Y., Lan, L., Chen, L., and Lu, J. (2013) Down-regulating overexpressed human Lon in cervical cancer suppresses cell proliferation and bioenergetics. *PLoS One* **8**, e81084

*Received for publication May 6, 2014.
Accepted for publication August 4, 2014.*